Electron spin resonance and nuclear magnetic resonance

2197055

Abstract. Electron spin resonance (ESR) and nuclear magnetic resonance (NMR) are two important spectroscopic techniques for probing properties of materials containing constituents with non-zero permanent magnetic moments capable of resonant absorption of electromagnetic energy — electronic systems in the case of ESR and atomic nuclei in the case of NMR. In this experiment, we studied ESR on a sample of Diphenyl-Picryl-Hydrazil (DPPH), a paramagnetic organic molecule with an unpaired e^-, by means of measuring the resonant frequency as a function of externally applied magnetic field, in order to determine the sample's g-factor, which was found to be $g_{\mathrm{DPPH}} = 2.02 \pm 0.01$. Further, we investigated the magnetic properties of ^{1}H and ^{19}F nuclei in the following substances: glycerine, polystyrene (both of which contain hydrogen), PTFE (which contains fluorine), and polythene, whose composition we wanted to learn about. The experimentally measured g-factors were $g_{\mathrm{glycerine}} = 5.54 \pm 0.03$, $g_{\mathrm{polystyrene}} = 5.68 \pm 0.01$ and $g_{\mathrm{PTFE}} = 5.34 \pm 0.01$. Comparison with the results obtained for polythene lead us to postulate the presence of hydrogen in our polythene sample, as confirmed by its chemical formula.

1. Introduction

Electron spin resonance (ESR), also referred to as electron paramagnetic resonance (EPR) spectroscopy, is an important method for studying paramagnetic chemical substances, in which the electrons' magnetic moments don't cancel, such as organic and inorganic free radicals or transition-metal ion complexes. It can provide detailed information relating to the chemical composition and structure of materials, and therefore finds innumerable applications in biology, chemistry, materials science, medicine and pharmacology, to name just a few.

Similarly, nuclear magnetic resonance (NMR) exploits the fact that some nuclei possess a non-zero overall spin, and hence a permanent magnetic moment, to probe the properties of materials containing such nuclei. It has widespread use and far-reaching applications, notably in medical imaging, where it forms the basis behind MRI (magnetic resonance imaging).

The aim of this experiment was to explore the fundamental principles underlying these two phenomena.

2. ESR

In the first part of the experiment, we performed an ESR study on a sample of Diphenyl-Picryl-Hydrazil (DPPH), which is a paramagnetic organic molecule with a single unpaired e^-. The orbital angular momentum of this electron is essentially zero, and hence the molecule's total magnetic moment is solely due to the electron's intrinsic spin angular momentum, which makes it particularly suited for ESR investigations.

2.1. Theory

In the absence of any external magnetic fields (i.e. for a free e^-), the two possible spin states ("spin up" and "spin down") are degenerate — they have the same energy.

However, *energy splitting* occurs when the electron is placed in a magnetic field. Indeed, the intrinsic spin gives rise to a magnetic moment $\boldsymbol{\mu}_S$ which interacts with the applied field and possesses a different energy depending on its relative spatial orientation.

According to quantum mechanics, only two configurations are possible. The magnitude S of the spin vector $\mathbf{S}$, and its two allowed z-components S_z (where the z-axis is defined to lie along the direction of the field), are respectively given by

$$\begin{aligned} S &= ||\mathbf{S}|| = \sqrt{s(s+1)}\hbar = \tfrac{\sqrt{3}}{2}\hbar, \quad \text{and} \\ S_z &= m_s\hbar. \end{aligned} \tag{2.1}$$

where $s = \frac{1}{2}$ is the spin quantum number, $m_s = \pm\frac{1}{2}$ is the secondary spin quantum number, and $\hbar = \frac{h}{2\pi}$ is the reduced Planck's constant.

The associated magnetic moment is

$$\boldsymbol{\mu}_S = -g\frac{\mu_B}{\hbar}\mathbf{S} \tag{2.2}$$

where g is the Landé splitting factor, or g-factor (which for a free electron has the value $g_e = 2.002319$), and $\mu_B = 9.274 \times 10^{-24}\,\mathrm{J\,T^{-1}}$ is the Bohr magneton.

A magnetic moment $\boldsymbol{\mu}_S$ in a field $\mathbf{B} = B\,\mathbf{e_z}$ (where $\mathbf{e_z}$ is the unit vector in the z-direction) has potential energy

$$E = -\boldsymbol{\mu}_S \cdot \mathbf{B} \underset{(2.2)}{=} -(-g\frac{\mu_B}{\hbar}\mathbf{S}) \cdot \mathbf{B} \underset{(2.1)}{=} g\frac{\mu_B}{\hbar}S_z B = g\mu_B m_s B. \tag{2.3}$$

Equation (2.3) shows that the two orientations ($m_s = \pm\frac{1}{2}$) no longer have the same energy — the one whose magnetic moment is aligned with the field (or equivalently whose spin points in the direction opposite to the field, i.e. $m_s = -\frac{1}{2}$) has a lower potential energy than the one whose magnetic moment is anti-parallel to the field, as depicted in figure 1. The energy difference between the two levels is

$$\Delta E = g\mu_B B. \tag{2.4}$$

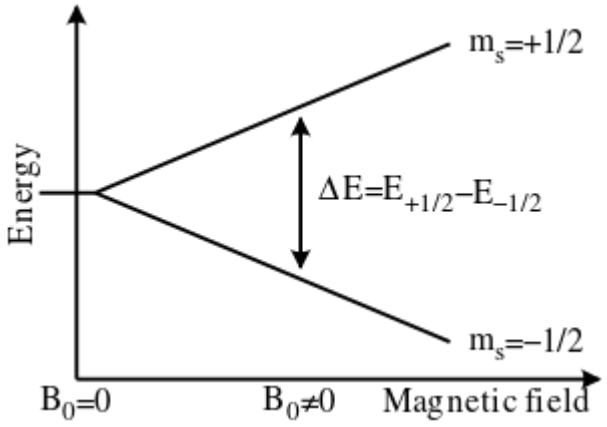

Figure 1. Energy splitting of the two spin states of an e^- placed in an external magnetic field $\mathbf{B_0}$.

In thermal equilibrium, the spins are distributed according to the Boltzmann distribution

$$\frac{N_{+\frac{1}{2}}}{N_{-\frac{1}{2}}} = \exp(-\frac{\Delta E}{k_B T}),$$

where k_B is Boltzmann's constant, and $N_{\pm\frac{1}{2}}$ are the number of spins in the higher and lower states, respectively.

If there is a predominance of spins in the lower state, transitions can be induced by supplying energy to the sample, for instance by irradiating it with electromagnetic (EM) radiation of the right frequency ν. The energy of an EM wave is $h\nu$, where h is Planck's constant, so the condition for resonance, using (2.4), can be stated as

$$h\nu = g\mu_B B. \tag{2.5}$$

In a real material, an electron "feels" also fields produced by any surrounding magnetic nuclei and/or other electrons, whose effect can be interpreted in terms of a shift in the g-factor compared to the free-electron value, and in this particular experiment, we were measuring the g-value of DPPH. In addition, the chemical environment also has an effect on the shape of the resonance signal and its line width, amongst other things, which gives an indication of how ESR can be used to infer information about the chemical composition and structure of materials.

2.2. Experimental method

A magnetic field was generated by two parallel vertically-positioned Helmholtz coils connected to a DC current supply. The DPPH sample was placed in the middle, wrapped inside another coil connected to an RF circuit oscillating at an adjustable frequency ν, providing energy in quanta of size $h\nu$. The magnetic field of the Helmholtz coils was varied by changing the current, keeping ν fixed, and resonance was detected with an oscilloscope thanks to an observable voltage change in the RF circuit signal that occurred each time the condition (2.5) was met. The measurement was repeated for a number of different frequencies.

For an e^- with only two possible spin states, it would be necessary to match the RF frequency and the current in the coils with considerable accuracy to obtain resonance. Furthermore, once the population of the spin states has been inverted, the sample can no longer absorb more energy before enough electrons have returned to the lower state, which means that the excitation rate needed to be slower than the *relaxation time* that it takes the electrons to return to thermal equilibrium via spin-spin and spin-lattice interactions.

A solution to both issues was to superimpose a (50Hz) modulation AC current on the DC component going into the coils, resulting in a sinusoidally-varying total field $\mathbf{B}_{total}(t)$ oscillating around a central value B_0. If the resonance condition (2.5) was satisfied for some value of $\mathbf{B}_{total}$ during this oscillation, a resonance signal was observed, twice during the cycle, at symmetric positions (provided that the phase lag between the modulation and the sample response was taken into account).

By adjusting the DC current, it was possible to make the resonance occur at the point in the cycle when the modulating field dropped to zero, so that it was precisely this B_0 that was satisfying the condition (2.5); and we performed a calibration of the coils, using a Hall probe sensor, to be able to deduce the value of B_0 from the DC current flowing through them, which was directly measurable.

2.3. Results

The relevant results are summarized in the following two subsections.

2.3.1. Helmholtz coils calibration. We varied the DC current in the Helmholtz coils and recorded the magnetic field at the centre. Since quite large fluctuations were observed in the field for a given current, 5 different readings were taken and averaged. For the purposes of error analysis, the uncertainty in the mean field was taken to be half the spread of the observed values, and for the current, half the smallest scale division.

We subsequently performed a weighted least-squares straight-line fit to the data. Figure 2 shows the resulting calibration curve with uncertainties indicated by error bars. The line of best fit was

$$B_0 = (3.73 \pm 0.01)I + (0.03 \pm 0.01),$$

where I is in Ampère, and B_0 in milliTesla. This equation was then used to convert between measured current and magnetic field applied to the sample. The MATLAB's built-in function `polyval` allowed us to estimate the uncertainties in the values of B_0 predicted by the curve, based on the goodness of fit.

2.3.2. Measurement of the g-factor of DPPH. The frequency in the RF oscillator circuit was varied in steps of 5 MHz, and for each one, the current in the coils was scanned over the range 0.1 A to 1.2 A to find the resonance. For a given frequency, the measurement was repeated multiple times to get an idea of the uncertainty involved. Figure 3 shows the resonant frequency as a function of the field.

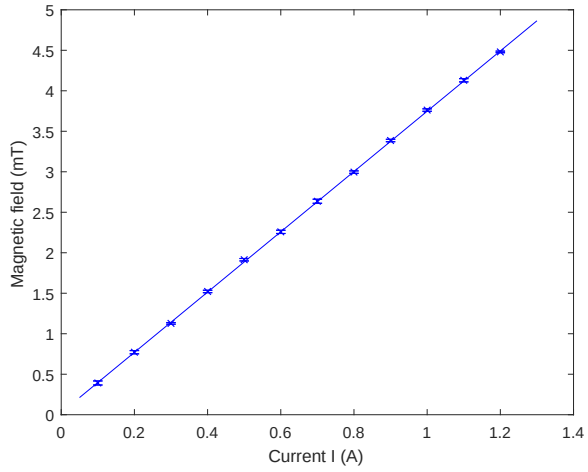

Figure 2. Magnetic field at the centre of the Helmholtz coils set-up as a function of the current passing through it.

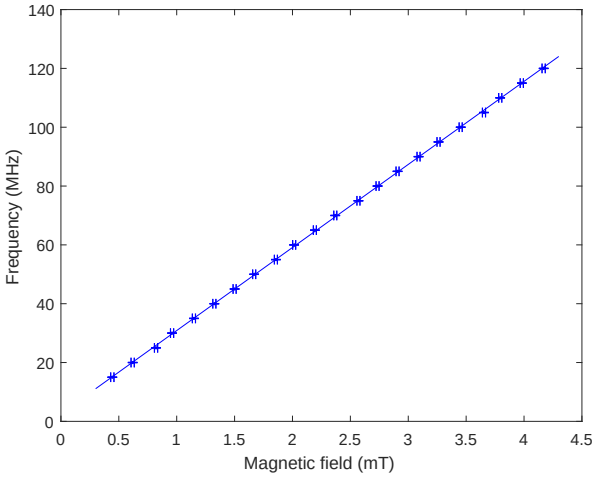

Figure 3. Resonant frequency as a function of the applied magnetic field for DPPH.

2.4. Analysis

According to equation (2.5), the plot of frequency ν against magnetic field B_0 should be a straight line with gradient

$$\frac{\nu}{B_0} = \frac{g_{\mathrm{DPPH}}\mu_B}{h},$$

which implies

$$g_{\mathrm{DPPH}} = \left(\frac{h}{\mu_B}\right)\left(\frac{\nu}{B_0}\right). \tag{2.6}$$

From the weighted straight-line fit to our data shown in figure 3, we had

$$\left(\frac{\nu}{B_0}\right) = 28.24 \pm 0.07\ \mathrm{MHz\,mT^{-1}}.$$

Substituting into (2.6) yielded

$$g_{\mathrm{DPPH}} = 2.02 \pm 0.01,$$

(where the uncertainty in the final value was computed, given that h and μ_B are constants, simply by multiplying the error in the gradient by h/μ_B).

2.5. Discussion

For a pair of Helmholtz coils separated by a distance equal to their radius, the theory of electromagnetism predicts that the value of the field at the centre should obey approximately

$$B_0 = \mu_0 \left(\frac{4}{5}\right)^{\frac{3}{2}} \frac{n}{r} I,$$

where $\mu = 4\pi \times 10^{-7}\ \mathrm{V\,s\,A^{-1}\,m^{-1}}$, n is the number of turns per coil, and r is their radius.

This shows that the expected relationship between I and B_0 is linear, as confirmed by our data (see figure 2). However, for our particular coils, the expected value of the gradient was 4.23, which does not agree with the one we obtained experimentally, i.e. 3.73 ± 0.01. This could be due to the fact that the separation of the coils might not have been exactly equal to their radius. Due to such possible differences in our set-up from the idealised case, we used the experimentally obtained calibration curve in subsequent calculations, not the theoretical one. Any error in the calibration curve therefore represents a systematic error in the results obtained thereafter.

Possible sources of error were the difficulty in making sure that the Hall probe was oriented perpendicularly to the measured field (i.e. parallel to the coils), and that it was located at the exact position where the sample was later placed. We also couldn't be sure whether the Hall probe itself was calibrated correctly (as we didn't obtain the expected result when we checked with a standard magnet), and whether we zeroed it at a point with no magnetic field. This could have introduced a systematic offset. A source of statistical errors were the random fluctuations in the magnetic field as well as in the response of the probe over time (e.g. due to warming up of the equipment or other reasons).

The accepted value for the g-factor of DPPH is

$$g_{\mathrm{DPPH,\ th}} = 2.0036.$$

Our value lies within 2σ of this value, and is therefore in reasonable agreement. Compare this with the theoretical value for the spin g-factor of a free e^-, which is

$$g_{e,\ \mathrm{th}} = 2.002319.$$

This is slightly different from both the accepted and our experimental value for g_{DPPH}, which, as explained in the section 2.1, could stem from the effect of the chemical surrounding of the unpaired e^-. Nevertheless, the values are relatively close, showing in particular that the assumption that we can neglect the orbital angular momentum of the e^-, and attribute the molecule's magnetic moment solely to the intrinsic spin is largely justified.

3. NMR

In the second part of the experiment, we performed NMR on protons and fluorine atoms in both liquid and solid samples, namely in glycerine and polystyrene (which contain ^{1}H), PTFE (containing ^{19}F), and polythene, about which we wanted to determine whether it is more likely to contain hydrogen or fluorine.

3.1. Theory

The basic principles of NMR are essentially the same as those of ESR. Atomic nuclei that have an odd number of nucleons can have a non-zero overall nuclear spin **S** which gives rise to a nuclear magnetic moment $\boldsymbol{\mu}_n$. When placed in a magnetic field, either external, or due to other close-by magnetic nuclei or the orbiting electrons, the nuclear spin can adopt, quantum-mechanically speaking, $2S + 1$ possible orientations, each corresponding to a different energy level

$$E_n = -g\mu_n B_0 n, \quad n = -S, -S+1, \ldots, 0, \ldots, S.$$

The g-factor again depends on the chemical environment and bond structure (so-called "chemical shift").

All of our samples had $S = \frac{1}{2}$, which meant there were only two possible spin levels, and the condition for resonance was

$$h\nu = \Delta E = -g\mu_n B_0. \tag{3.1}$$

3.2. Experimental method

The experimental procedure was analogous to the ESR part of the experiment (see section (2.2)). The only differences were that the static magnetic field was generated by an iron-cored electromagnet, instead of Helmholtz coils, and the modulating field was produced by a pair of smaller attached modulation coils.

3.3. Results

3.3.1. Electromagnet calibration. Just like in section 2.3.1, we first calibrated the electromagnet to be able to relate the current passing through it to the magnetic field it generates. Since the electromagnet contained an iron core, its field depended not only the value of the current, but also on whether the current was being increased or decreased. This effect is called *hysteresis* (a dependence of the net magnetization of a ferromagnet on the history of any externally applied magnetic field).

Therefore, we did our calibration first for an increasing and then a decreasing current. Figure 4 shows the hysteresis curve that we obtained.

Note. *Only the part of the curve corresponding to increasing current was used in the next section.*

We fitted a polynomial of degree 2, $y = ax^2 + bx + c$, to the upper half of the curve (this was the degree that yielded the lowest error estimates on the fit parameters), with

$$\begin{aligned} a &\approx -16 \pm 1, \\ b &\approx 189 \pm 7, \\ c &\approx -34 \pm 12. \end{aligned}$$

3.3.2. Measurement of the g-factors of Glycerine, Polystyrene and PTFE. Figure 5 shows the graphs of resonance frequencies as a function of B_0 for the 3 different substances.

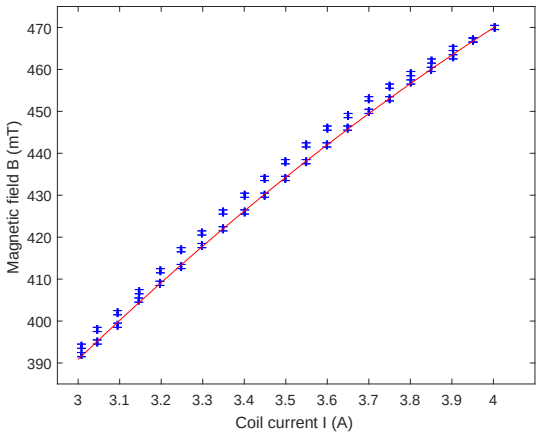

Figure 4. Magnetic field inside the electromagnet as a function of the current.

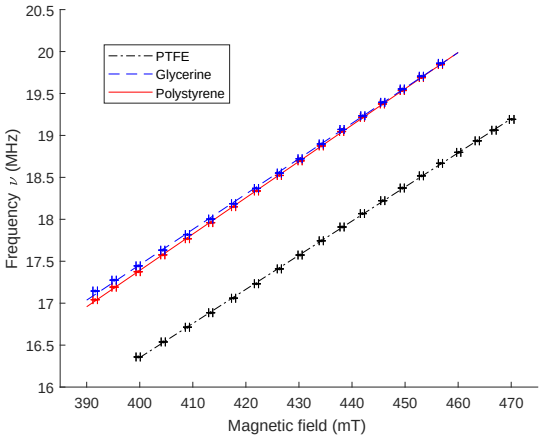

Figure 5. Resonant frequency as a function of applied magnetic field for glycerine, polystyrene and PTFE

3.4. Analysis

According to (3.1), $\left|\frac{\nu}{B_0}\right|$ should be a constant, equal to $\frac{g\mu_n}{h}$. It follows that $g = \frac{h}{\mu_n}\left(\frac{\nu}{B_0}\right)$. We performed a straight-line fit to our plots in figure 5, and got

$$\left(\frac{\nu}{B_0}\right)_{\text{glycerine}} = 0.0422 \pm 0.0002 \text{ MHz mT}^{-1}$$
$$g_{\text{glycerine}} = 5.54 \pm 0.03$$

$$\left(\frac{\nu}{B_0}\right)_{\text{polystyrene}} = 0.0433 \pm 0.0001 \text{ MHz mT}^{-1}$$
$$g_{\text{polystyrene}} = 5.68 \pm 0.01$$

$$\left(\frac{\nu}{B_0}\right)_{\text{PTFE}} = 0.0407 \pm 0.0001 \text{ MHz mT}^{-1}$$
$$g_{\text{PTFE}} = 5.34 \pm 0.01$$

3.5. Discussion

4. Conclusion

Our measurements of resonant absorption confirmed the linear relationship predicted by (2.5) and (3.1) between the magnetic field and the resonance frequency. They showed that, indeed, in both ESR and NMR, an energy splitting occurs when the sample is placed in an external field, that this creates separate energy levels such that the energy difference between them scales linearly with the applied field, and that energy transitions can be induced by supplying EM energy of the correct frequency.

An increase in the precision of our findings could have been achieved by taking further repeated measurements, as the statistical errors due to random fluctuations were quite significant, but also by using stronger **B** fields, thus increasing the energy differences between the spin states and reducing the relative uncertainty, and/or by operating at lower temperatures,

both of which would have potentially resulted in sharper resonance signals with a reduced line width.

References

[1]